

---

# DPBridge: Latent Diffusion Bridge for Dense Prediction

---

Haorui Ji<sup>1</sup> Taojun Lin<sup>1</sup> Hongdong Li<sup>1</sup>

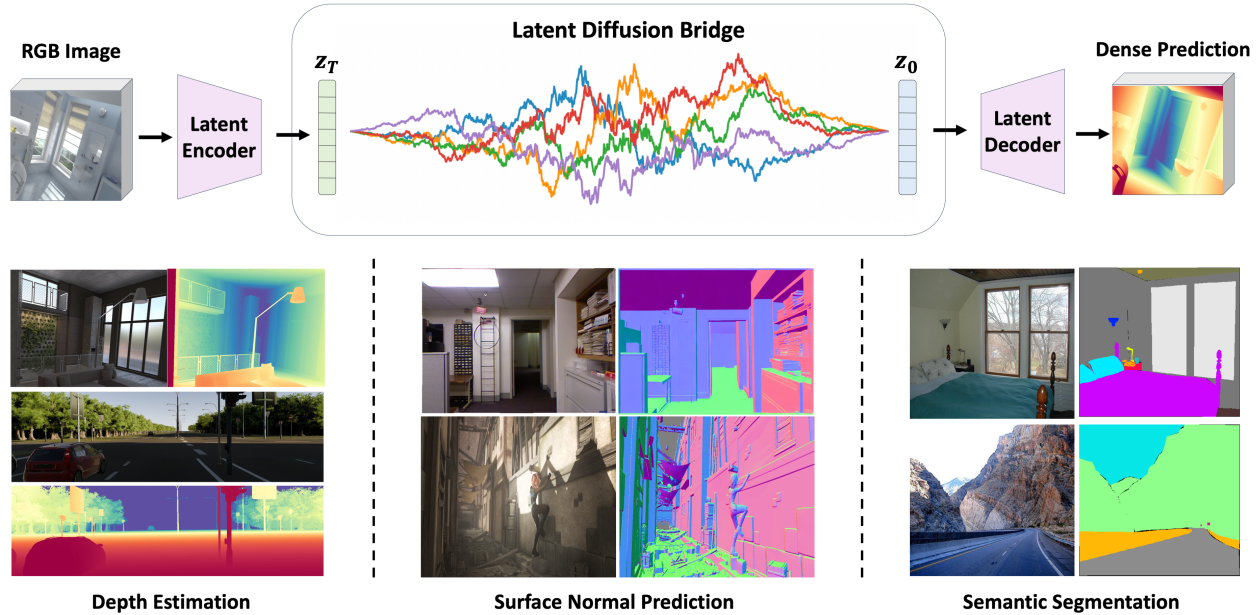


Figure 1: We present **DPBridge** to tackle general dense prediction tasks by establishing conditional probability transport between RGB images and corresponding dense maps in the latent space based on a tractable diffusion bridge process. In addition, we introduce finetuning strategies to adapt large pretrained diffusion backbone to construct our bridge, leveraging its rich prior knowledge to enable both efficient training and robust generalization.

## Abstract

Diffusion models have shown remarkable capabilities in modeling complex data distributions by transforming noise into structured data through stochastic processes. However, when applied to dense prediction tasks whose goal is to capture per-pixel relationships between RGB images and dense signal maps, starting the sampling process from an uninformative Gaussian noise often leads to inefficient sampling and long latency. To overcome these challenges, we propose DPBridge, a generative framework that establishes direct mapping between input RGB images and dense signal maps based on a tractable bridge process. Furthermore, we introduce finetuning strategies to leverage a pretrained large-scale image diffusion backbone, enjoying its rich visual prior knowledge to enable both efficient training and robust generalization. Experiments show that

DPBridge achieves competitive performance compared to both feed-forward and diffusion-based approaches across various benchmarks, validating its effectiveness and adaptability.

## 1. Introduction

Dense prediction refers to the type of problems whose primary goal is to assign a value at every spatial location in the input data, generating output signal maps that possess same structure and size as inputs. It incorporates various typical tasks, including depth estimation (Yang et al., 2024; Ranftl et al., 2021; Eftekhar et al., 2021), surface normal prediction (Bae & Davison, 2024; Hu et al., 2024; Bae et al., 2021), semantic segmentation (Chen, 2017; Cheng et al., 2022; Wang et al., 2023; Weber et al., 2021), optical flow (Teed & Deng, 2020; Huang et al., 2022; Weinzaepfel et al., 2023), etc.

Recently, image diffusion models have been applied to dense prediction tasks by formulating them as conditional generation problems. Their ability to capture complex data distributions makes them effective priors, leading to highly favorable results (Ke et al., 2024; Garcia et al., 2024; Fu et al., 2025). Following a common practice, these methods diffuse signal maps into pure noise and subsequently leverage input RGB images as conditions to guide the generation process. Nonetheless, there still exists limitations in diffusion-based solutions, mostly stem from the underlying modeling mechanism. The denoising process of a standard diffusion model always starts from Gaussian noise, which contains little information about the target signal distribution. In such cases, the distance between prior Gaussian distribution and target distribution remains large, requiring inevitably more sampling steps as well as ad-hoc conditioning mechanisms, at the risk of degraded performance and prolonged convergence time.

Instead of starting from noise, one feasible alternative is to directly initiate the generative process from input RGB images, as they are structurally correlated to target signal maps and can naturally serve as more informative prior. This leads to the exploration of a new family of computational frameworks, i.e. diffusion bridge models (Liu et al., 2022; Zhou et al., 2023; Li et al., 2023; Liu et al., 2023). They are based on stochastic process with fixed starting and ending points and are adept at modeling conditional probability paths. By establishing direct connections between different distributions, this line of framework provides a more natural and efficient way to model probability transport compared with previous efforts by reducing the dependence on manually designed post-hoc guidance (Chung et al., 2022a; Song et al., 2023; Chung et al., 2022b) or customized generation pipeline (Meng et al., 2021). We therefore advocate that adopting diffusion bridge model will be a better fit to dense prediction tasks compared with conventional diffusion-based counterparts.

Motivated by this, we propose **Dense Prediction Bridge (DPBridge)**, a latent diffusion bridge model to handle general dense prediction tasks through generative pipeline. In essence, we modify the standard diffusion process to directly bridge the latents of RGB images and corresponding dense signal maps, and enforce the model to learn this process through maximum likelihood estimation. In this way the generative process thus becomes a series of transformations that iteratively synthesize desired signal maps starting from RGB images rather than pure noise, enabling faster inference speed as well as better generation quality.

Furthermore, we introduce novel finetuning strategies to better adapt pretrained diffusion backbone to DPBridge construction. The equipped rich visual prior not only helps boosting the perception performance as well as general-

ization capability, but also significantly speeds up training convergence. Figure 1 is a high-level overview of DPBridge, while also demonstrating its effectiveness on three representative dense prediction tasks, i.e. depth estimation, surface normal prediction, and semantic segmentation, proving that our framework is theoretically universal and can be instantiated to different scenarios.

To summarize, our contributions are as follows:

- We propose the DPBridge framework to address dense prediction tasks within a generative pipeline by formulating them as instances of latent diffusion bridges.
- We propose finetuning strategies to effectively adapt large pretrained backbone to diffusion bridges, allowing for exploitation of visual prior knowledge and training efficiency improvements.
- Our proposed method exhibits competitive performance across different tasks in terms of both quantitative metrics and visual inspection, highlighting its effectiveness and generalization capability.

## 2. Related Works

### 2.1. Dense Prediction

Dense predictions can be characterized as a conditional distribution modeling task and common solutions can be categorized into discriminative and generative ones. Discriminative methods directly map input data to structured outputs in a feed-forward manner. (Ranftl et al., 2021) introduces attention mechanism and transformer architecture to better capture both local and global context feature. (Yang et al., 2024) explore the usage of large-scale synthetic and pseudo-labeled images to enhance model’s capacity and robustness. (Bae & Davison, 2024) incorporates per-pixel ray directions and models the relative rotations between neighboring pixels. Recently, diffusion-based generative models have been applied in this field and showed remarkable performance. (Ke et al., 2024) finetunes pretrained diffusion model, leveraging the rich visual knowledge within to enhance depth estimation. (Fu et al., 2025) takes advantage of diffusion priors to jointly estimate depth and surface normals from single image, enhancing detail preservation by decoupling complex data distributions into distinct sub-distributions. (Gui et al., 2024) exploits flow matching to facilitate the distribution shift between images and depth maps. Our work follow conventional generative pipeline, but instead of starting from pure noise, we establish direct connections between input image and target signal map distributions, and model conditional probability transport in iterative denoising manner.

## 2.2. Diffusion and Bridge Models

Diffusion models (Ho et al., 2020; Song et al., 2020b) are a family of generative models that are able to capture complex data distributions through a sequence of forward and reverse processes. They accelerate the development of modern generative systems, and have consistently obtained state-of-the-art performance across various domains, such as image and video synthesis (Rombach et al., 2022; Ho et al., 2022), controlled editing (Zhang et al., 2023; Batzolis et al., 2021), inverse problem solving (Chung et al., 2022a; Song et al., 2023), 3D assets generation (Xiang et al., 2024; Zhang et al., 2024), and human-centered applications (Ji et al., 2024b; Ji & Li, 2024).

Diffusion bridge models have gained increasing attention in generative modeling in recent years (Liu et al., 2022; Zhou et al., 2023; Liu & Wu, 2023; De Bortoli et al., 2021). They offer a novel perspective for translating between different distributions and enable a more effective data-to-data generation paradigm. Recent works have explored different types of bridge processes and their applications. (Liu et al., 2023; Li et al., 2023; Yue et al., 2023) develop Schrödinger bridge, Brownian bridge, and Ornstein-Uhlenbeck bridge frameworks, applying them to image restoration tasks such as inpainting, super-resolution. (Chung et al., 2024) proposes a modified inference procedure that enforces data consistency. (Chen et al., 2023) introduces bridge models to text-to-speech systems, enhancing synthesis quality and sampling efficiency. To the best of our knowledge, no prior work has explored the use of bridge models for dense prediction tasks to facilitate distribution transport between images and dense signal maps, despite their structural closeness. Our work aims to address this research gap.

## 3. Preliminary

### 3.1. Diffusion Process

A diffusion process  $\mathbb{Q} = \{\mathbf{z}_t \in \mathbb{R}^d : t \in [0, T]\}$  on space  $\mathbb{R}^d$  follows the stochastic differential equation of form

$$d\mathbf{z}_t = f(\mathbf{z}_t, t)dt + g(t)d\mathbf{w}_t \quad (1)$$

where  $\mathbf{w}_t$  is a standard Wiener process,  $f : \mathbb{R}^d \times [0, T] \rightarrow \mathbb{R}$  and  $g : [0, T] \rightarrow \mathbb{R}$  are the drift and diffusion coefficients that describe the evolution of this stochastic process. The transition kernel is specified as  $q(\mathbf{z}_t|\mathbf{z}_0) = \mathcal{N}(\alpha_t\mathbf{z}_0, \sigma_t^2\mathbf{I})$  and the noise schedule comprising differentiable functions  $\alpha_t, \sigma_t$  depends on the design choice of drift and diffusion coefficients. It is also common to assess the diffusion process in terms of the signal-to-noise ratio (SNR), defined as  $\text{SNR}_t = \alpha_t^2/\sigma_t^2$ .

### 3.2. Diffusion Bridge Process

Diffusion bridge process is a special type of diffusion process that is conditioned to end at a specified terminal point at timestep  $T$ . One natural way of its construction is to derive the conditioned process from a reference diffusion process given terminal constraints. We can use Doob’s h-transform technique (Oksendal, 2013; Särkkä & Solin, 2019) to modify a reference process  $\mathbb{Q}$  defined in Equation (1) to ensure that the event  $\mathbf{z}_T = \mathbf{x}$  happens, where  $\mathbf{x}$  is a predefined value. The conditioned process  $\mathbb{Q}^{\mathbf{x}}(\cdot) := \mathbb{Q}(\cdot|\mathbf{z}_T = \mathbf{x})$  thus follows the law of

$$d\mathbf{z}_t = [f(\mathbf{z}_t, t) + g^2(t)h(\mathbf{z}_t, t, \mathbf{x}, T)] dt + g(t)d\mathbf{w}_t \quad (2)$$

where  $h(\mathbf{z}_t, t, \mathbf{x}, T) = \nabla_{\mathbf{z}_t} \log q(\mathbf{z}_T = \mathbf{x}|\mathbf{z}_t)$ . Intuitively, the additional drift term  $h(\mathbf{z}_t, t, \mathbf{x}, T)$  plays the role of steering  $\mathbf{z}_t$  towards the target point  $\mathbf{z}_T = \mathbf{x}$ , and it is ensured that  $\mathbb{Q}^{\mathbf{x}}$  invariably passes  $\mathbf{x}$  at timestep  $T$  with probability 1 for any initial point  $\mathbf{z}_0$ .

The transition kernel of  $\mathbb{Q}^{\mathbf{x}}$ , given by  $q(\mathbf{z}_t|\mathbf{z}_0, \mathbf{z}_T)$ , can be subsequently derived through Kolmogorov equation:

$$\begin{aligned} q(\mathbf{z}_t|\mathbf{z}_0, \mathbf{z}_T) &= \mathcal{N}(m_t\mathbf{z}_0 + n_t\mathbf{z}_T, \sigma_t^2\mathbf{I}) \\ m_t &= \alpha_t \left( 1 - \frac{\text{SNR}_T}{\text{SNR}_t} \right) \\ n_t &= \frac{\text{SNR}_T}{\text{SNR}_t} \frac{\alpha_t}{\alpha_T} \\ \sigma_t &= \sigma_t \sqrt{1 - \frac{\text{SNR}_T}{\text{SNR}_t}}, \end{aligned} \quad (3)$$

where  $\text{SNR}_t, \alpha_t, \sigma_t^2$  are all ingredients defined in the reference process  $\mathbb{Q}$ .

## 4. Method

### 4.1. Problem Formulation

We formulate different dense prediction tasks as instances of image-conditioned generation problems and propose DPBridge to model the conditional distributions  $p(\mathbf{y}|\mathbf{x})$ , where  $\mathbf{y} \in \mathbb{R}^{H \times W \times C}$  indicates the desired dense signal map (e.g. depth, surface normal, segmentation map), and  $\mathbf{x} \in \mathbb{R}^{H \times W \times 3}$  is the input RGB image. In the following sections, we’ll elaborate the details of DPBridge framework, which is constructed based on pretrained diffusion backbone through proper finetuning.

### 4.2. Dense Prediction Bridge

Given paired training data, a naive implementation is to construct the diffusion bridge model from scratch according to Section 3.2. However, this approach is extremely resource-demanding, making it hard to implement with limited computation power. What’s more, it lacks the ability to harness

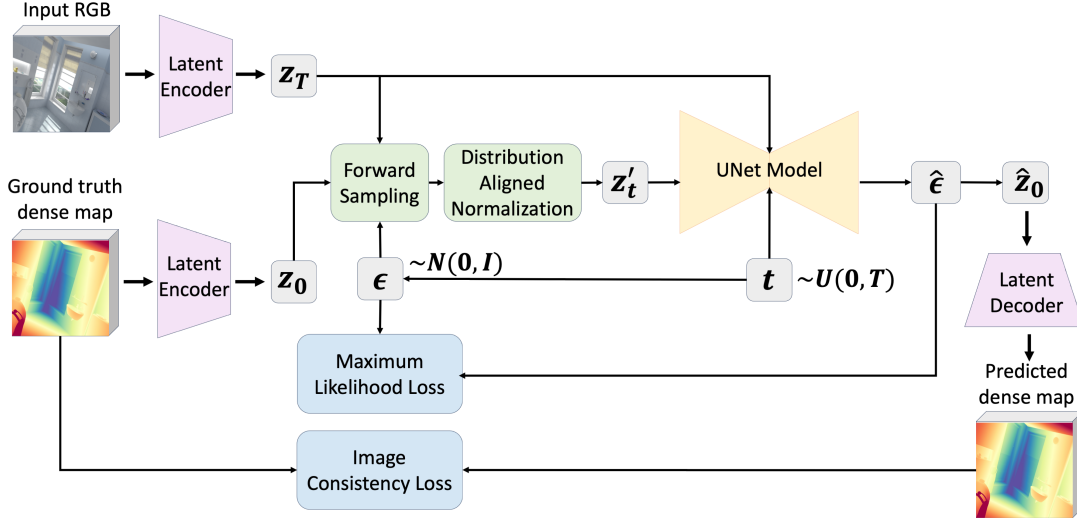


Figure 2: Overview of our training pipeline. To overcome the discrepancy with standard diffusion process and facilitate finetuning, we derive the maximum likelihood training objective of diffusion bridge process, propose a distribution aligned normalization strategy, and assist the training with an auxiliary image consistency loss.

rich visual prior knowledge inherent in the foundation models, which have been proven significant in terms of boosting both perception quality and generalization performance in dense prediction tasks. Therefore, our DPBridge is build upon pretrained diffusion backbones through finetuning and we explore several strategies to handle the misalignment between bridge process and standard diffusion process, aiming for more efficient knowledge transfer. Figure 2 gives an overview of the proposed finetuning pipeline, and next we’ll explain the design of each component.

### 4.3. Latent Space Implementation

Instead of directly learning in image pixel space, we follow common practice to perform diffusion steps in a compressed but perceptually aligned latent space, provided by an independently trained variational autoencoder (VAE). Specifically, both the dense signal maps and RGB images are converted by the encoder to obtain  $\mathbf{z}_0 = \mathcal{E}(\mathbf{y})$  and  $\mathbf{z}_T = \mathcal{E}(\mathbf{x})$ , serving as the initial and terminal points. In this way the diffusion bridge process is henceforth learned in the latent space. To retrieve original signal map we can use the decoder to decode the predicted latents  $\mathbf{y} = \mathcal{D}(\hat{\mathbf{z}}_0)$ . In later part of this paper, with little abuse of notation, all derivations are conducted in the latent space.

### 4.4. Training Objective

#### 4.4.1. MAXIMUM LIKELIHOOD LOSS

Widely-used techniques for learning the reverse process that corresponds to Equation (2) is to follow the theory of (Anderson, 1982), use a neural network to approximate the score function and apply score matching. We notice that analytical form of diffusion bridge’s reverse transition kernel

is directly obtainable, therefore the usage of maximum likelihood training can also be applied, which is performed by optimizing the Evidence Lower Bound (ELBO). It yields a more stable loss function compared with score matching and better aligns with the pretrained backbone. Given the specified terminal state  $\mathbf{z}_T$ , the expectation of data log-likelihood possesses the following ELBO formulation:

$$ELBO = \mathbb{E}_{p(\mathbf{z}_0)} \left[ \mathbb{E}_{p(\mathbf{z}_1|\mathbf{z}_0)} \left[ \log p_\theta(\mathbf{z}_0 | \mathbf{z}_1, \mathbf{z}_T) \right] - \sum_{t=2}^T \mathbb{E}_{p(\mathbf{z}_t|\mathbf{z}_0)} \left[ \mathbb{D}_{KL} (q(\mathbf{z}_{t-1} | \mathbf{z}_0, \mathbf{z}_t, \mathbf{z}_T) || p_\theta(\mathbf{z}_{t-1} | \mathbf{z}_t, \mathbf{z}_T)) \right] \right] \quad (4)$$

where  $q(\mathbf{z}_{t-1}|\mathbf{z}_t, \mathbf{z}_0, \mathbf{z}_T)$  and  $p_\theta(\mathbf{z}_{t-1}|\mathbf{z}_t, \mathbf{z}_T)$  are the transition kernel of true reverse process and our modeled generative process and  $\mathbb{D}_{KL}$  is the KL divergence. Utilizing Bayes’ theorem and Markov chain property, we can obtain:

$$q(\mathbf{z}_{t-1}|\mathbf{z}_t, \mathbf{z}_0, \mathbf{z}_T) = \frac{q(\mathbf{z}_t|\mathbf{z}_{t-1}, \mathbf{z}_T)q(\mathbf{z}_{t-1}|\mathbf{z}_0, \mathbf{z}_T)}{q(\mathbf{z}_t|\mathbf{z}_0, \mathbf{z}_T)} = \mathcal{N}(\tilde{\boldsymbol{\mu}}_t(\mathbf{z}_t, \mathbf{z}_0, \mathbf{z}_T), \tilde{\boldsymbol{\sigma}}_t^2 \mathbf{I}) \quad (5)$$

For simplicity, we define the following notations:  $a_t = m_t/m_{t-1}$ ,  $b_t = n_t - a_t \cdot n_{t-1}$ ,  $\delta_t^2 = \sigma_t^2 - a_t^2 \cdot \sigma_{t-1}^2$ . The mean value term is:

$$\begin{aligned} \tilde{\boldsymbol{\mu}}_t(\mathbf{z}_t, \mathbf{z}_0, \mathbf{z}_T) &= k_1 \mathbf{z}_t + k_2 \mathbf{z}_0 + k_3 \mathbf{z}_T \\ k_1 &= \frac{\sigma_{t-1}^2}{\sigma_t^2} \cdot a_t \\ k_2 &= \frac{\delta_t^2}{\sigma_t^2} \cdot m_{t-1} \\ k_3 &= \frac{\delta_t^2}{\sigma_t^2} \cdot n_{t-1} - \frac{\sigma_{t-1}^2}{\sigma_t^2} \cdot a_t \cdot b_t, \end{aligned} \quad (6)$$

and the variance is:

$$\tilde{\sigma}_t^2 = \frac{\sigma_{t-1}^2}{\sigma_t^2} \cdot \delta_t^2 \quad (7)$$

Assume  $p_\theta(\mathbf{z}_{t-1}|\mathbf{z}_t, \mathbf{z}_T)$  is also a Gaussian distribution parameterized as  $\mathcal{N}(\boldsymbol{\mu}_\theta(\mathbf{z}_t, \mathbf{z}_T, t), \boldsymbol{\Sigma}_\theta(\mathbf{z}_t, \mathbf{z}_T, t))$  and let  $\boldsymbol{\Sigma}_\theta(\mathbf{z}_t, \mathbf{z}_T, t) = \tilde{\sigma}_t^2$  for derivation simplicity, maximizing the ELBO is equivalent to minimizing:

$$\mathcal{L}_{elbo} = \mathbb{E}_{t, \mathbf{z}_0, \mathbf{z}_t, \mathbf{z}_T} \left[ \frac{1}{2\tilde{\sigma}_t^2} \|\hat{\boldsymbol{\mu}}_t - \boldsymbol{\mu}_\theta(\mathbf{z}_t, \mathbf{z}_T, t)\|^2 \right] \quad (8)$$

Similar to the strategy in DDPM (Ho et al., 2020), we use a network  $\epsilon_\theta(\mathbf{z}_t, \mathbf{z}_T, t)$  to parameterize noise instead of posterior mean and further simplified the loss as:

$$\mathcal{L}_{elbo} = \mathbb{E}_{t, \mathbf{z}_0, \mathbf{z}_t, \mathbf{z}_T} \left[ \|\epsilon - \epsilon_\theta(\mathbf{z}_t, \mathbf{z}_T, t)\|^2 \right], \quad (9)$$

#### 4.4.2. IMAGE CONSISTENCY LOSS

In addition to the likelihood loss evaluated in latent space, we also incorporate an image-level consistency loss, where we first convert the latent prediction back to image space, and then evaluate its consistency with the ground truth dense map using a simple MSE loss.

$$\mathcal{L}_{ic} = \|\mathcal{D}(\hat{\mathbf{z}}_0) - \mathbf{y}\|^2 \quad (10)$$

The reason is that the compression of input data in the latent space will lead to a loss of high-frequency information, harming the model’s ability of preserving fine-grained spatial details. By introducing an auxiliary loss at image level, we ensure that the model is capable of retaining spatial information which is essential for precise per-pixel prediction. This dual loss strategy leverages the compactness of latent space for efficiency while still anchoring the training process to the fidelity of full-resolution dense map prediction, thus leading to performance improvement. Combined these two losses together, our final training objective becomes:

$$\mathcal{L} = \omega_1 \mathcal{L}_{elbo} + \omega_2 \mathcal{L}_{ic} \quad (11)$$

where  $\omega_1, \omega_2$  are hyperparameters to balance the loss.

#### 4.5. Distribution Alignment Normalization

A notable challenge during finetuning is the misalignment of intermediate sample’s marginal distribution  $q(\mathbf{z}_t)$  between DPBridge and diffusion backbone, due to the difference in the forward transition kernel. This misalignment will weaken the model’s inherent denoising ability, thus limiting the effectiveness of knowledge transfer. To address this issue, we propose a distribution alignment normalization technique to fill in the gap between the two distributions. Specifically, we normalize the intermediate latents computed from Equation (3) to match the form of a standard diffusion process:

$$\mathbf{z}'_t = \frac{\mathbf{z}_t - m_t \mathbf{z}_T}{\sqrt{n_t^2 + \sigma_t^2}} = \frac{n_t}{\sqrt{n_t^2 + \sigma_t^2}} \mathbf{z}_0 + \frac{\sigma_t}{\sqrt{n_t^2 + \sigma_t^2}} \boldsymbol{\epsilon}_t \quad (12)$$

---

#### Algorithm 1 Training

---

**Require:** Encoder  $\mathcal{E}$ ; Decoder  $\mathcal{D}$ ; Loss weights  $\omega_1, \omega_2$

- 1: **repeat**
  - 2:   Retrieve paired data  $(\mathbf{x}, \mathbf{y})$
  - 3:    $\mathbf{z}_0 = \mathcal{E}(\mathbf{y}), \mathbf{z}_T = \mathcal{E}(\mathbf{x})$
  - 4:    $t \sim \text{Uniform}(\{1, \dots, T\}), \epsilon \sim \mathcal{N}(\mathbf{0}, \mathbf{I})$
  - 5:    $\mathbf{z}_t = m_t \mathbf{z}_0 + n_t \mathbf{z}_T + \sigma_t \epsilon$
  - 6:    $\mathbf{z}'_t = \frac{1}{\sqrt{n_t^2 + \sigma_t^2}} (\mathbf{z}_t - n_t \mathbf{z}_T)$
  - 7:    $\mathcal{L}_{elbo} = \|\epsilon - \epsilon_\theta(\mathbf{z}'_t, \mathbf{z}_T, t)\|^2$ ,
  - 8:    $\hat{\mathbf{z}}_0 = \frac{1}{m_t} (\mathbf{z}_t - n_t \mathbf{z}_T - \sigma_t \epsilon_\theta(\mathbf{z}'_t, \mathbf{z}_T, t))$
  - 9:    $\mathcal{L}_{ic} = \|\mathcal{D}(\hat{\mathbf{z}}_0) - \mathbf{y}\|^2$
  - 10:   Take gradient step on  $\nabla_\theta (\omega_1 \mathcal{L}_{elbo} + \omega_2 \mathcal{L}_{ic})$
  - 11: **until Converged**
- 

---

#### Algorithm 2 Inference

---

**Require:** Encoder  $\mathcal{E}$ ; Decoder  $\mathcal{D}$ ; Trained  $\epsilon_\theta(\cdot, \cdot, \cdot)$

- 1:  $\mathbf{z}_T = \mathcal{E}(\mathbf{x})$
  - 2: **for**  $t = T, \dots, 1$  **do**
  - 3:    $\epsilon \sim \mathcal{N}(\mathbf{0}, \mathbf{I})$  if  $t > 1$ , else  $\epsilon = \mathbf{0}$
  - 4:    $\mathbf{z}'_t = \frac{1}{\sqrt{n_t^2 + \sigma_t^2}} (\mathbf{z}_t - n_t \mathbf{z}_T)$
  - 5:    $\hat{\mathbf{z}}_0 = \frac{1}{m_t} (\mathbf{z}_t - n_t \mathbf{z}_T - \sigma_t \epsilon_\theta(\mathbf{z}'_t, \mathbf{z}_T, t))$
  - 6:    $\mathbf{z}_{t-1} = k_1 \mathbf{z}_t + k_2 \hat{\mathbf{z}}_0 + k_3 \mathbf{z}_T + \tilde{\sigma}_t \epsilon$
  - 7: **end for**
  - 8:  $\mathbf{y} = \mathcal{D}(\hat{\mathbf{z}}_0)$
  - 9: **return**  $\mathbf{y}$
- 

Since the square sum of coefficients is equal to 1, the normalized bridge process  $\{\mathbf{z}'_t : t \in [0, T]\}$  is the same as a standard VP process, making the marginal distribution of these two aligned. Therefore by feeding the normalized sample  $\mathbf{z}'_t$  in the network  $\epsilon_\theta$ , we can fully exploit the denoising capability from pretrained diffusion backbone. An overview of DPBridge’s training pipeline shown in Algorithm 1.

#### 4.6. Accelerate Inference

Similar to the idea of DDIM (Song et al., 2020a), the inference process of DPBridge can be accelerated by utilizing a non-Markovian process while maintaining the same marginal distributions for all intermediate samples along the sampling path. Specifically, we can sample on a subset of timesteps  $\{t_i\}_{i=1}^N$ , where  $0 = t_0 < t_1 < \dots < t_{N-1} < t_N = T$  and the number of sampling steps  $N$  can be set independently from the original timesteps  $T$  on which the bridge model is trained. The accelerated inference process can be thus described as:

$$\mathbf{z}_{t_n} = m_{t_n} \hat{\mathbf{z}}_0 + n_{t_n} \mathbf{z}_T + \sqrt{\sigma_{t_n}^2 - g_n^2} \frac{\mathbf{z}_{t_{n+1}} - m_{t_{n+1}} \hat{\mathbf{z}}_0 - n_{t_{n+1}} \mathbf{z}_T}{\sigma_{t_{n+1}}} + g_n \boldsymbol{\epsilon} \quad (13)$$

where  $g_n$  is the variance parameter that controls the stochasticity behavior of the reverse sampling process. We note that when  $g_n = \tilde{\sigma}_t^2$  which is calculated from Equation (5), the process becomes a Markovian bridge. The basic inference process of DPBridge is summarized in Algorithm 2. If adopt acceleration, one can utilize Equation (13) during implementation.

## 5. Experiments

We conduct evaluation mainly on two representative dense prediction tasks, i.e., depth estimation and surface normal prediction. We’ll start by a brief introduction of experiment settings as well as implementation details, followed by quantitative and qualitative analysis. Lastly, we conduct detailed ablation studies and investigate the influence each design component respectively.

### 5.1. Experiments Setup

**Datasets.** The basic setting for depth estimation and surface normal prediction experiments are similar. We use two synthetic datasets, HyperSim (Roberts et al., 2021) and Virtual KITTI (Cabon et al., 2020), which cover both indoor and outdoor scenes, for training. To comprehensively evaluate the model performance and demonstrate its generalization capability, we conduct zero-shot evaluations on real-world datasets. For depth estimation, this includes NYUv2 (Silberman et al., 2012), KITTI (Geiger et al., 2012), ScanNet (Dai et al., 2017), ETH3D (Schops et al., 2017) and DIODE (Vasiljevic et al., 2019). For surface normal prediction, we additionally incorporate iBims (Koch et al., 2018) and Sintel (Butler et al., 2012) datasets. For fair comparison, we use the same validation split as in previous methods (Ke et al., 2024).

**Evaluation Metrics.** For depth estimation, we follow the affine-invariant evaluation protocol, where we first align the prediction results to the ground truth with least squares fitting, and then use Absolute Mean Relative Error (AbsRel) and  $\delta_1$  accuracy to assess the performance. Denote the ground truth depth  $\mathbf{d}$ , predicted depth  $\hat{\mathbf{d}}$ , and the number of valid pixels  $N$ , the AbsRel is calculated as  $\frac{1}{N} \sum_{i=1}^N \|\mathbf{d}_i - \hat{\mathbf{d}}_i\|/\mathbf{d}_i$ , and  $\delta_1$  accuracy is measured using the ratio of pixels satisfying  $\max(\mathbf{d}_i/\hat{\mathbf{d}}_i, \hat{\mathbf{d}}_i/\mathbf{d}_i) < 1.25$ . For the metrics of surface normal task, we report the commonly used mean angular error between the ground-truth normal vectors and the prediction results, as well as the percentage of pixels with an angular error below 11.25 degrees.

### 5.2. Implementation Details

We implement DPBridge based on Stable Diffusion v1.5 (SD1.5) and v2.1-base (SD2.1) (Rombach et al., 2022) and report their results respectively to shown compatibility

with different backbones. During training, the number of timesteps of is set to be 1000, and we use 50 sampling steps during inference with considerations of both quality and efficiency. Training our method takes 30K iterations using the Adam optimizer with a base learning rate of  $3 \times 10^{-5}$  and an exponential decay strategy after 100-step warm-up. The batch size is 2, but with 8 steps gradient accumulation, the effective batch size is equivalent to 16. We also apply random horizontal flipping augmentation during training. The whole process takes approximately 3 days to complete on a single Nvidia RTX 3090Ti GPU.

### 5.3. Quantitative and Qualitative Results

Table 1 and Table 2 summarize the quantitative metrics of DPBridge compared with state-of-the-art (SOTA) methods from both discriminative and generative fields, all in zero-shot manner. In depth estimation, DPBridge consistently matches SOTA results, while demonstrating robust generalization across datasets. It achieves 4.4 AbsRel, 97.2%  $\delta_1$  on NYUv2, and 4.5 AbsRel, 97.4%  $\delta_1$  on ScanNet. Similarly, for surface normal prediction, DPBridge also delivers competitive results, achieving mean error of 14.8 and 11.25° accuracy of 65.3% on NYUv2, as well as maintaining strong performance on other datasets like iBims-1 (mean: 17.1, 11.25° : 68.0%) and Sintel (mean: 25.0, 11.25° : 46.3%). These results highlight DPBridge’s versatility to generalize well across tasks and benchmarks, being comparable to both feed-forward and diffusion-based methods while offering a unified, efficient paradigm to handle dense prediction tasks. Notably, when compared with bridge models like I2SB and BBDM that are trained from scratch, we exceed their performance by a large margin, justifying our proposal that adapting prior knowledge to bridge construction indeed benefits the perception performance. In terms of diffusion-based methods, DPBridge can also achieve the best result, showcasing that adopting bridge process to handle dense prediction tasks is indeed advantageous over standard diffusion framework.

We further provide qualitative examples for both tasks in comparison with SOTA diffusion-based methods (Ke et al., 2024; Fu et al., 2025; Garcia et al., 2024), which are most closely related to our work. Figure 3 shows that E2E-FT tends to produce blurry and smooth predictions, while Geowizard fails to provide accurate estimation in relatively long distance range. In contrast, DPBridge perform well in both indoor and outdoor scenes, capturing fine-level details in both near and faraway regions, like the contour of leaves, fences, cars, computers or windows. Figure 4 presents visualizations on in-the-wild images for surface normal prediction task, where we can see that DPBridge is able to predict high-quality surface normals equipped with fine-grained textures.

Submission and Formatting Instructions for ICML 2025

Method	Model Type			NYUv2		KITTI		ETH3D		ScanNet		DIODE		Avg. Rank
	FF	DM	BM	AbsRel↓	$\delta_1$ ↑	AbsRel↓	$\delta_1$ ↑							
DiverseDepth (Yin et al., 2020)	✓			11.7	87.5	19.0	70.4	22.8	69.4	10.9	88.2	37.6	63.1	12.4
MiDaS (Ranftl et al., 2020)	✓			11.1	88.5	23.6	63.0	18.4	75.2	12.1	84.6	33.2	71.5	11.8
LeReS (Yin et al., 2021)	✓			9.0	91.6	14.9	78.4	17.1	77.7	9.1	91.1	27.1	76.6	9.5
Omnidata (Eftekhari et al., 2021)	✓			7.4	94.5	14.9	83.5	16.6	77.8	7.5	93.2	33.9	74.2	9.2
HDN (Zhang et al., 2022)	✓			6.9	94.8	11.5	86.7	12.1	83.3	8.0	93.6	24.6	78.0	7.2
DPT (Ranftl et al., 2021)	✓			9.8	90.3	10.0	90.1	7.8	94.6	8.2	93.8	18.2	75.8	6.9
Depth Anything V2 (Yang et al., 2024)	✓			<b>4.4</b>	<b>97.9</b>	<b>7.5</b>	<b>94.8</b>	13.2	84.2	<b>4.4</b>	<b>98.0</b>	<b>6.5</b>	<b>95.4</b>	<b>2.3</b>
Marigold (Ke et al., 2024)		✓		6.0	95.9	10.5	90.4	7.1	<u>95.1</u>	6.9	94.5	31.0	71.2	5.8
DepthFM (Gui et al., 2024)		✓		6.5	95.6	<u>8.3</u>	<u>93.4</u>	-	-	-	-	<u>22.5</u>	80.0	3.8
Geowizard (Fu et al., 2025)		✓		5.7	96.2	14.4	82.0	7.5	94.3	6.1	95.8	31.4	77.1	6.1
E2E-FT (Garcia et al., 2024)		✓		5.4	96.4	9.6	92.1	<b>6.4</b>	<b>95.9</b>	5.8	96.5	30.3	77.6	3.4
I2SB (Liu et al., 2023)			✓	24.9	73.4	37.7	57.9	40.6	52.0	21.2	66.1	40.2	59.1	13.9
BBDM (Li et al., 2023)			✓	27.9	65.5	47.2	45.1	46.4	48.8	22.7	67.0	34.6	64.7	14.1
<b>DPBridge (SD1.5)</b>			✓	6.9	95.7	11.2	87.3	8.1	93.2	7.5	94.7	29.7	78.6	6.1
<b>DPBridge (SD2.1)</b>			✓	<b>4.4</b>	<u>97.6</u>	9.8	91.6	<u>6.9</u>	94.9	<u>4.5</u>	<u>97.4</u>	23.8	<u>84.0</u>	<u>2.6</u>

Table 1: Quantitative comparison of DPBridge with state-of-the-art affine-invariant depth estimation methods on zero-shot benchmarks. All metrics are presented in percentage terms. FF, DM, and BM correspond to feed-forward, diffusion models, and bridge models. The best and second-best results are highlighted in **bold** and underline formats.

Method	Model Type			NYUv2		ScanNet		iBims-1		Sintel		Avg. Rank
	FF	DM	BM	Mean↓	11.25° ↑							
EESNU (Bae et al., 2021)	✓			<u>16.2</u>	58.6	-	-	20.0	58.5	42.1	11.5	6.5
Omnidata v1 (Eftekhari et al., 2021)	✓			23.1	45.8	22.9	47.4	19.0	62.1	41.5	11.4	8.1
Omnidata v2 (Kar et al., 2022)	✓			17.2	55.5	16.2	60.2	18.2	63.9	40.5	14.7	5.6
DSINE (Bae & Davison, 2024)	✓			16.4	59.6	16.2	61.0	17.1	67.4	34.9	21.5	3.2
Marigold (Ke et al., 2024)		✓		18.8	55.9	17.7	58.8	18.4	64.3	39.1	14.9	5.8
Geowizard (Fu et al., 2025)		✓		17.0	56.5	15.4	61.6	<b>13.0</b>	65.3	40.4	13.2	4.1
E2E-FT (Garcia et al., 2024)		✓		16.5	<u>60.4</u>	<u>14.7</u>	<u>66.1</u>	<u>16.1</u>	<b>69.7</b>	<u>33.5</u>	<u>22.3</u>	<u>2.1</u>
<b>DPBridge (SD1.5)</b>			✓	18.1	54.2	18.0	54.5	24.3	51.2	41.2	19.4	7.3
<b>DPBridge (SD2.1)</b>			✓	<b>14.8</b>	<b>65.3</b>	<b>13.4</b>	<b>68.5</b>	17.1	<u>68.0</u>	<b>25.0</b>	<b>46.3</b>	<b>1.4</b>

Table 2: Quantitative comparison of DPBridge with state-of-the-art surface normal prediction methods on zero-shot benchmarks. All metrics are presented in percentage terms. FF, DM, and BM correspond to feed-forward, diffusion models, and bridge models. The best and second-best results are highlighted in **bold** and underline formats.

Design Components			NYUv2		KITTI	
<i>FT</i>	<i>DAN</i>	<i>IC</i>	AbsRel↓	$\delta_1$ ↑	AbsRel↓	$\delta_1$ ↑
	✓	✓	21.8	83.7	30.6	62.7
✓			6.4	94.0	11.2	87.0
✓		✓	6.2	95.8	11.0	87.5
✓	✓		5.0	96.3	10.3	90.1
✓	✓	✓	4.4	97.6	9.8	91.6

Table 3: Ablation studies regarding different design components. *FT* stands for finetuning pretrained backbone. *DAN* denotes distribution aligned normalization technique. *IC* indicates image consistency loss.

#### 5.4. Ablation Studies

To evaluate the effectiveness of each design component and training setting, we conduct ablation studies using depth estimation tasks on the NYUv2 and KITTI datasets. The results are summarized in Table 3 and Figure 5, with detailed discussions provided below.

**Finetuning VS Training From Scratch.** To assess whether adapting pretrained diffusion backbones improves perception performance, we conduct comparison between finetuning and training from scratch paradigm. As shown in the first row of Table 3, fine-tuning significantly outperforms training from scratch under identical experimental settings. This difference is due to two factors: first, foundation models trained on large, diverse datasets. They capture universal visual priors, aiding knowledge transfer to dense prediction tasks. Second, training from scratch requires more iterations for convergence. In addition, from the last two rows of Table 1 and Table 2, we can see that finetuning on SD2.1 exceeds that on SD1.5, suggesting that the quality of prior knowledge will also influence the performance. These observations indicate that building DPBridge on superior pretrained backbones is indeed advantageous.

**Distribution Alignment Normalization.** Next, we evaluate whether aligning the marginal distributions between diffusion bridge process and standard diffusion process is

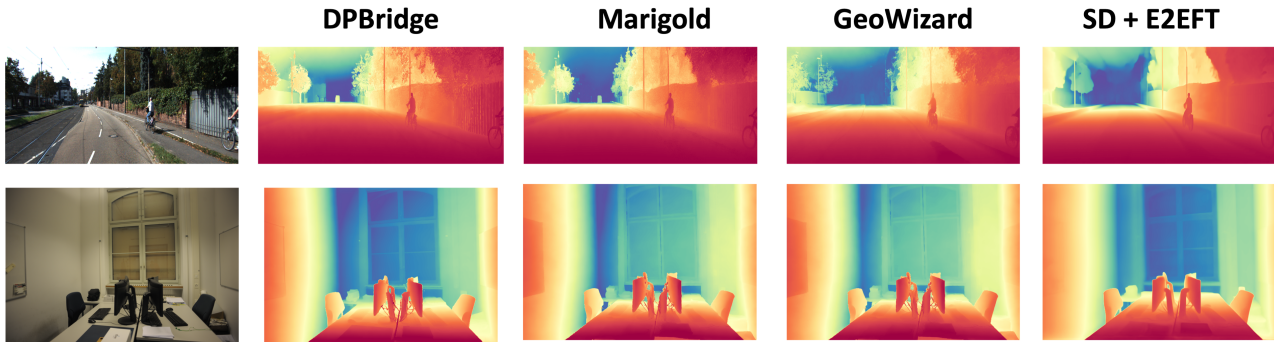


Figure 3: Qualitative comparison of diffusion-based depth estimation methods on KITTI and ETH3D dataset. DPBridge is able to generalize in both indoor and outdoor scenes, successively capturing fine-grained details such as leaves and structures on the fence (KITTI).

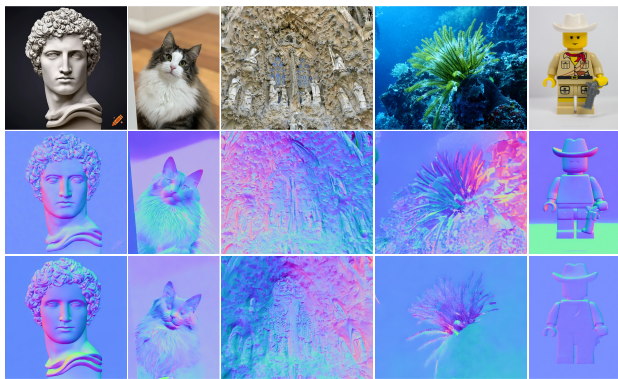


Figure 4: Qualitative comparison between DPBridge (above) and Marigold (below) on normal estimation results, DPBridge is able to capture more textures from the photos in-the-wild.

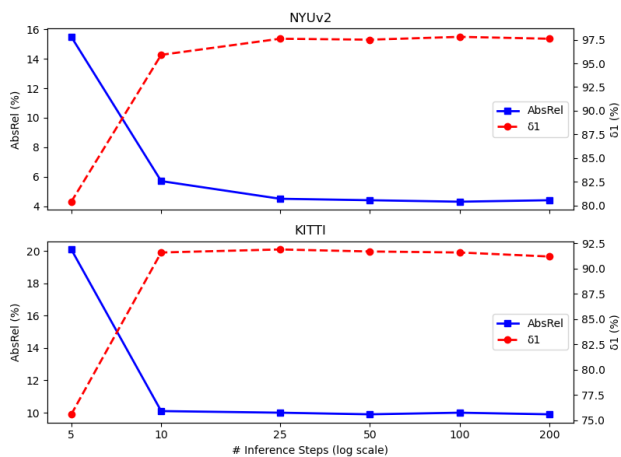


Figure 5: Ablation of sampling steps. The performance improves as the number of sampling steps increases, while we observe saturation after 10 steps.

beneficial. As shown in the second and fourth rows of Table 3, incorporating a distribution alignment normalization step before inputting data into the noise prediction network noticeably improves performance.

**Image Consistency Loss.** Regarding the auxiliary image consistency loss, the comparison between the third and fourth rows in Table 3 shows that while effective, its impact is less significant than that of distribution alignment normalization. This is probably because it primarily influences regions where masked and valid areas overlap, which constitute only a relatively small proportion of the data. However, when integrated with other design components, the overall performance is significantly improved.

**Number of Sampling Steps.** We evaluate performance with varying numbers of sampling steps during inference. As shown in Figure 5, increasing sampling steps initially improves perception performance rapidly and reach saturation after 10 steps. Notably, compared to the results in Table 1, where all other diffusion-based methods are evaluated with 50 steps setting, DPBridge achieves comparable performance with fewer steps, demonstrating the efficiency of our proposed method.

## 6. Conclusion

In this paper, we present DPBridge, a latent diffusion bridge model to tackle general dense prediction tasks through generative pipeline. We establish direct mapping between input images and corresponding signal maps in the latent space based on fully-tractable diffusion bridge process. In this way, the prior distribution is no longer constrained to uninformative noise, but instead can be chosen as more structurally correlated ones. In addition, we introduce effective finetuning strategies to adapt large pretrained diffusion backbone to our bridge model construction, leveraging its rich prior knowledge to boost training speed and achieve remarkable perception performance. Future research directions include deriving other parameterization of diffusion bridge process, and extending to more dense prediction tasks.

## Impact Statement

This paper presents work whose goal is to advance the field of Machine Learning and we wish to spark further research on image generation and perception. There are many potential societal consequences of our work, none which we feel must be specifically highlighted here.

## References

- Anderson, B. D. Reverse-time diffusion equation models. *Stochastic Processes and their Applications*, 12(3):313–326, 1982.
- Bae, G. and Davison, A. J. Rethinking inductive biases for surface normal estimation. In *Proceedings of the IEEE/CVF Conference on Computer Vision and Pattern Recognition*, pp. 9535–9545, 2024.
- Bae, G., Budvytis, I., and Cipolla, R. Estimating and exploiting the aleatoric uncertainty in surface normal estimation. In *Proceedings of the IEEE/CVF International Conference on Computer Vision*, pp. 13137–13146, 2021.
- Batzolis, G., Stanczuk, J., Schönlieb, C.-B., and Etmann, C. Conditional image generation with score-based diffusion models. *arXiv preprint arXiv:2111.13606*, 2021.
- Butler, D. J., Wulff, J., Stanley, G. B., and Black, M. J. A naturalistic open source movie for optical flow evaluation. In *Computer Vision—ECCV 2012: 12th European Conference on Computer Vision, Florence, Italy, October 7–13, 2012, Proceedings, Part VI 12*, pp. 611–625. Springer, 2012.
- Cabon, Y., Murray, N., and Humenberger, M. Virtual kitti 2. *arXiv preprint arXiv:2001.10773*, 2020.
- Chen, L.-C. Rethinking atrous convolution for semantic image segmentation. *arXiv preprint arXiv:1706.05587*, 2017.
- Chen, Z., He, G., Zheng, K., Tan, X., and Zhu, J. Schrödinger bridges beat diffusion models on text-to-speech synthesis. *arXiv preprint arXiv:2312.03491*, 2023.
- Cheng, B., Misra, I., Schwing, A. G., Kirillov, A., and Girdhar, R. Masked-attention mask transformer for universal image segmentation. In *Proceedings of the IEEE/CVF conference on computer vision and pattern recognition*, pp. 1290–1299, 2022.
- Chung, H., Kim, J., Mccann, M. T., Klasky, M. L., and Ye, J. C. Diffusion posterior sampling for general noisy inverse problems. *arXiv preprint arXiv:2209.14687*, 2022a.
- Chung, H., Sim, B., Ryu, D., and Ye, J. C. Improving diffusion models for inverse problems using manifold constraints. *Advances in Neural Information Processing Systems*, 35:25683–25696, 2022b.
- Chung, H., Kim, J., and Ye, J. C. Direct diffusion bridge using data consistency for inverse problems. *Advances in Neural Information Processing Systems*, 36, 2024.
- Cordts, M., Omran, M., Ramos, S., Rehfeld, T., Enzweiler, M., Benenson, R., Franke, U., Roth, S., and Schiele, B. The cityscapes dataset for semantic urban scene understanding. In *Proceedings of the IEEE conference on computer vision and pattern recognition*, pp. 3213–3223, 2016.
- Dai, A., Chang, A. X., Savva, M., Halber, M., Funkhouser, T., and Nießner, M. Scannet: Richly-annotated 3d reconstructions of indoor scenes. In *Proceedings of the IEEE conference on computer vision and pattern recognition*, pp. 5828–5839, 2017.
- De Bortoli, V., Thornton, J., Heng, J., and Doucet, A. Diffusion schrödinger bridge with applications to score-based generative modeling. *Advances in Neural Information Processing Systems*, 34:17695–17709, 2021.
- Eftekhari, A., Sax, A., Malik, J., and Zamir, A. Omnidata: A scalable pipeline for making multi-task mid-level vision datasets from 3d scans. In *Proceedings of the IEEE/CVF International Conference on Computer Vision*, pp. 10786–10796, 2021.
- Fu, X., Yin, W., Hu, M., Wang, K., Ma, Y., Tan, P., Shen, S., Lin, D., and Long, X. Geowizard: Unleashing the diffusion priors for 3d geometry estimation from a single image. In *European Conference on Computer Vision*, pp. 241–258. Springer, 2025.
- Garcia, G. M., Zeid, K. A., Schmidt, C., de Geus, D., Hermans, A., and Leibe, B. Fine-tuning image-conditional diffusion models is easier than you think. *arXiv preprint arXiv:2409.11355*, 2024.
- Geiger, A., Lenz, P., and Urtasun, R. Are we ready for autonomous driving? the kitti vision benchmark suite. In *2012 IEEE conference on computer vision and pattern recognition*, pp. 3354–3361. IEEE, 2012.
- Gui, M., Fischer, J. S., Prestel, U., Ma, P., Kotovenko, D., Grebenkova, O., Baumann, S. A., Hu, V. T., and Ommer, B. Depthfm: Fast monocular depth estimation with flow matching. *arXiv preprint arXiv:2403.13788*, 2024.
- Ho, J., Jain, A., and Abbeel, P. Denoising diffusion probabilistic models. *Advances in neural information processing systems*, 33:6840–6851, 2020.
- Ho, J., Salimans, T., Gritsenko, A., Chan, W., Norouzi, M., and Fleet, D. J. Video diffusion models. *arXiv:2204.03458*, 2022.

- Hu, M., Yin, W., Zhang, C., Cai, Z., Long, X., Chen, H., Wang, K., Yu, G., Shen, C., and Shen, S. Metric3d v2: A versatile monocular geometric foundation model for zero-shot metric depth and surface normal estimation. *arXiv preprint arXiv:2404.15506*, 2024.
- Huang, Z., Shi, X., Zhang, C., Wang, Q., Cheung, K. C., Qin, H., Dai, J., and Li, H. Flowformer: A transformer architecture for optical flow. In *European conference on computer vision*, pp. 668–685. Springer, 2022.
- Ji, H. and Li, H. 3d human pose analysis via diffusion synthesis. *arXiv preprint arXiv:2401.08930*, 2024.
- Ji, H., Deng, H., Dai, Y., and Li, H. Unsupervised 3d pose estimation with non-rigid structure-from-motion modeling. In *Proceedings of the IEEE/CVF Winter Conference on Applications of Computer Vision*, pp. 3314–3323, 2024a.
- Ji, H., Wang, R., Lin, T., and Li, H. Jade: Joint-aware latent diffusion for 3d human generative modeling. *arXiv preprint arXiv:2412.20470*, 2024b.
- Kar, O. F., Yeo, T., Atanov, A., and Zamir, A. 3d common corruptions and data augmentation. In *Proceedings of the IEEE/CVF Conference on Computer Vision and Pattern Recognition*, pp. 18963–18974, 2022.
- Ke, B., Obukhov, A., Huang, S., Metzger, N., Daudt, R. C., and Schindler, K. Repurposing diffusion-based image generators for monocular depth estimation. In *Proceedings of the IEEE/CVF Conference on Computer Vision and Pattern Recognition*, pp. 9492–9502, 2024.
- Koch, T., Liebel, L., Fraundorfer, F., and Korner, M. Evaluation of cnn-based single-image depth estimation methods. In *Proceedings of the European Conference on Computer Vision (ECCV) Workshops*, pp. 0–0, 2018.
- Lee, C.-H., Liu, Z., Wu, L., and Luo, P. Maskgan: Towards diverse and interactive facial image manipulation. In *Proceedings of the IEEE/CVF conference on computer vision and pattern recognition*, pp. 5549–5558, 2020.
- Li, B., Xue, K., Liu, B., and Lai, Y.-K. Bbdm: Image-to-image translation with brownian bridge diffusion models. In *Proceedings of the IEEE/CVF conference on computer vision and pattern recognition*, pp. 1952–1961, 2023.
- Liu, G.-H., Vahdat, A., Huang, D.-A., Theodorou, E. A., Nie, W., and Anandkumar, A. I<sup>2</sup>sb: Image-to-image schrödinger bridge. *arXiv preprint arXiv:2302.05872*, 2023.
- Liu, X. and Wu, L. Learning diffusion bridges on constrained domains. In *international conference on learning representations (ICLR)*, 2023.
- Liu, X., Wu, L., Ye, M., and Liu, Q. Let us build bridges: Understanding and extending diffusion generative models. *arXiv preprint arXiv:2208.14699*, 2022.
- Meng, C., He, Y., Song, Y., Song, J., Wu, J., Zhu, J.-Y., and Ermon, S. Sdedit: Guided image synthesis and editing with stochastic differential equations. *arXiv preprint arXiv:2108.01073*, 2021.
- Oksendal, B. *Stochastic differential equations: an introduction with applications*. Springer Science & Business Media, 2013.
- Ranftl, R., Lasinger, K., Hafner, D., Schindler, K., and Koltun, V. Towards robust monocular depth estimation: Mixing datasets for zero-shot cross-dataset transfer. *IEEE transactions on pattern analysis and machine intelligence*, 44(3):1623–1637, 2020.
- Ranftl, R., Bochkovskiy, A., and Koltun, V. Vision transformers for dense prediction. In *Proceedings of the IEEE/CVF international conference on computer vision*, pp. 12179–12188, 2021.
- Roberts, M., Ramapuram, J., Ranjan, A., Kumar, A., Bautista, M. A., Paczan, N., Webb, R., and Susskind, J. M. Hypersim: A photorealistic synthetic dataset for holistic indoor scene understanding. In *Proceedings of the IEEE/CVF international conference on computer vision*, pp. 10912–10922, 2021.
- Rombach, R., Blattmann, A., Lorenz, D., Esser, P., and Ommer, B. High-resolution image synthesis with latent diffusion models. In *Proceedings of the IEEE/CVF conference on computer vision and pattern recognition*, pp. 10684–10695, 2022.
- Särkkä, S. and Solin, A. *Applied stochastic differential equations*, volume 10. Cambridge University Press, 2019.
- Schops, T., Schonberger, J. L., Galliani, S., Sattler, T., Schindler, K., Pollefeys, M., and Geiger, A. A multi-view stereo benchmark with high-resolution images and multi-camera videos. In *Proceedings of the IEEE conference on computer vision and pattern recognition*, pp. 3260–3269, 2017.
- Silberman, N., Hoiem, D., Kohli, P., and Fergus, R. Indoor segmentation and support inference from rgb-d images. In *Computer Vision—ECCV 2012: 12th European Conference on Computer Vision, Florence, Italy, October 7–13, 2012, Proceedings, Part V 12*, pp. 746–760. Springer, 2012.
- Song, J., Meng, C., and Ermon, S. Denoising diffusion implicit models. *arXiv preprint arXiv:2010.02502*, 2020a.

- Song, J., Vahdat, A., Mardani, M., and Kautz, J. Pseudoinverse-guided diffusion models for inverse problems. In *International Conference on Learning Representations*, 2023.
- Song, Y., Sohl-Dickstein, J., Kingma, D. P., Kumar, A., Ermon, S., and Poole, B. Score-based generative modeling through stochastic differential equations. *arXiv preprint arXiv:2011.13456*, 2020b.
- Sxela. <https://github.com/sxela/face2comics>. <https://github.com/Sxela/face2comics>, 2021.
- Teed, Z. and Deng, J. Raft: Recurrent all-pairs field transforms for optical flow. In *Computer Vision—ECCV 2020: 16th European Conference, Glasgow, UK, August 23–28, 2020, Proceedings, Part II 16*, pp. 402–419. Springer, 2020.
- Vasiljevic, I., Kolkin, N., Zhang, S., Luo, R., Wang, H., Dai, F. Z., Daniele, A. F., Mostajabi, M., Basart, S., Walter, M. R., et al. Diode: A dense indoor and outdoor depth dataset. *arXiv preprint arXiv:1908.00463*, 2019.
- Wang, X., Wang, W., Cao, Y., Shen, C., and Huang, T. Images speak in images: A generalist painter for in-context visual learning. In *Proceedings of the IEEE/CVF Conference on Computer Vision and Pattern Recognition*, pp. 6830–6839, 2023.
- Weber, M., Xie, J., Collins, M., Zhu, Y., Voigtlaender, P., Adam, H., Green, B., Geiger, A., Leibe, B., Cremers, D., et al. Step: Segmenting and tracking every pixel. *arXiv preprint arXiv:2102.11859*, 2021.
- Weinzaepfel, P., Lucas, T., Leroy, V., Cabon, Y., Arora, V., Brégier, R., Csurka, G., Antsfeld, L., Chidlovskii, B., and Revaud, J. Croco v2: Improved cross-view completion pre-training for stereo matching and optical flow. In *Proceedings of the IEEE/CVF International Conference on Computer Vision*, pp. 17969–17980, 2023.
- Xiang, J., Lv, Z., Xu, S., Deng, Y., Wang, R., Zhang, B., Chen, D., Tong, X., and Yang, J. Structured 3d latents for scalable and versatile 3d generation. *arXiv preprint arXiv:2412.01506*, 2024.
- Yang, L., Kang, B., Huang, Z., Zhao, Z., Xu, X., Feng, J., and Zhao, H. Depth anything v2. *arXiv preprint arXiv:2406.09414*, 2024.
- Yin, W., Wang, X., Shen, C., Liu, Y., Tian, Z., Xu, S., Sun, C., and Renyin, D. Diversedepth: Affine-invariant depth prediction using diverse data. *arXiv preprint arXiv:2002.00569*, 2020.
- Yin, W., Zhang, J., Wang, O., Niklaus, S., Mai, L., Chen, S., and Shen, C. Learning to recover 3d scene shape from a single image. In *Proceedings of the IEEE/CVF Conference on Computer Vision and Pattern Recognition*, pp. 204–213, 2021.
- Yue, C., Peng, Z., Ma, J., Du, S., Wei, P., and Zhang, D. Image restoration through generalized ornstein-uhlenbeck bridge. *arXiv preprint arXiv:2312.10299*, 2023.
- Zhang, C., Yin, W., Wang, B., Yu, G., Fu, B., and Shen, C. Hierarchical normalization for robust monocular depth estimation. *Advances in Neural Information Processing Systems*, 35:14128–14139, 2022.
- Zhang, L., Rao, A., and Agrawala, M. Adding conditional control to text-to-image diffusion models. In *Proceedings of the IEEE/CVF International Conference on Computer Vision*, pp. 3836–3847, 2023.
- Zhang, L., Wang, Z., Zhang, Q., Qiu, Q., Pang, A., Jiang, H., Yang, W., Xu, L., and Yu, J. Clay: A controllable large-scale generative model for creating high-quality 3d assets. *ACM Transactions on Graphics (TOG)*, 43(4): 1–20, 2024.
- Zhou, L., Lou, A., Khanna, S., and Ermon, S. Denoising diffusion bridge models. *arXiv preprint arXiv:2309.16948*, 2023.

In the supplementary material, we'll provide contents that are not included in the main paper due to page limitations. We first fill in the derivation details of the loss function. Afterwards we will provide the additional quantitative comparisons with more baseline methods. Finally, we will present qualitative examples that apply DPBridge on more dense prediction tasks.

## A. Derivation Details

In this section, we'll provide derivation details of the maximum likelihood loss presented in Section 4.4.1. Its core is the posterior distribution  $q(\mathbf{z}_{t-1}|\mathbf{z}_t, \mathbf{z}_0, \mathbf{z}_T)$  as in Equation (5), whose calculation involves three terms:  $q(\mathbf{z}_t|\mathbf{z}_{t-1}, \mathbf{z}_T)$ ,  $q(\mathbf{z}_{t-1}|\mathbf{z}_0, \mathbf{z}_T)$ , and  $q(\mathbf{z}_t|\mathbf{z}_0, \mathbf{z}_T)$ . The last two term of the posterior can be retrieved directly through the marginal distribution of diffusion bridge's forward process, but further derivation is required for the first term. Specifically, as specified in Equation (3):

$$\begin{aligned} q(\mathbf{z}_t|\mathbf{z}_0, \mathbf{z}_T) &= \mathcal{N}(m_t\mathbf{z}_0 + n_t\mathbf{z}_T, \sigma_t^2\mathbf{I}) \\ \mathbf{z}_t &= m_t\mathbf{z}_0 + n_t\mathbf{z}_T + \sigma_t\epsilon_t \end{aligned} \quad (14)$$

$$\begin{aligned} q(\mathbf{z}_{t-1}|\mathbf{z}_0, \mathbf{z}_T) &= \mathcal{N}(m_{t-1}\mathbf{z}_0 + n_{t-1}\mathbf{z}_T, \sigma_{t-1}^2\mathbf{I}) \\ \mathbf{z}_{t-1} &= m_{t-1}\mathbf{z}_0 + n_{t-1}\mathbf{z}_T + \sigma_{t-1}\epsilon_{t-1} \end{aligned} \quad (15)$$

To derive the transition probability  $q(\mathbf{z}_t|\mathbf{z}_{t-1}, \mathbf{z}_T)$ , we substitute  $\mathbf{z}_0$  in Equation (14) with derivation from Equation (15), obtain

$$\begin{aligned} \mathbf{z}_t &= a_t\mathbf{z}_{t-1} + b_t\mathbf{z}_T + \delta_t\epsilon \\ a_t &= \frac{m_t}{m_{t-1}} \\ b_t &= n_t - \frac{m_t}{m_{t-1}}n_{t-1} = n_t - a_t n_{t-1} \\ \delta_t^2 &= \sigma_t^2 - \frac{m_t}{m_{t-1}}n_{t-1}^2\sigma_{t-1}^2 = \sigma_t^2 - a_t^2\sigma_{t-1}^2 \end{aligned} \quad (16)$$

Thus, we can get  $q(\mathbf{z}_t|\mathbf{z}_{t-1}, \mathbf{z}_T) = \mathcal{N}(a_t\mathbf{z}_{t-1} + b_t\mathbf{z}_T, \delta_t^2\mathbf{I})$ , which is also a Gaussian distribution.

Putting all these terms back to Equation (5), we'll have:

$$\begin{aligned} q(\mathbf{z}_{t-1}|\mathbf{z}_t, \mathbf{z}_0, \mathbf{z}_T) &\sim \mathcal{N}(\tilde{\boldsymbol{\mu}}_t(\mathbf{z}_t, \mathbf{z}_0, \mathbf{z}_T), \tilde{\sigma}_t^2\mathbf{I}) \\ &= \frac{q(\mathbf{z}_t|\mathbf{z}_{t-1}, \mathbf{z}_T)q(\mathbf{z}_{t-1}|\mathbf{z}_0, \mathbf{z}_T)}{q(\mathbf{z}_t|\mathbf{z}_0, \mathbf{z}_T)} \\ &\propto \exp \left[ -\frac{1}{2} \left( \frac{(\mathbf{z}_t - a_t\mathbf{z}_{t-1} - b_t\mathbf{z}_T)^2}{\delta_t^2} + \frac{(\mathbf{z}_{t-1} - m_{t-1}\mathbf{z}_0 - n_{t-1}\mathbf{z}_T)^2}{\sigma_{t-1}^2} - \frac{(\mathbf{z}_t - m_t\mathbf{z}_0 - n_t\mathbf{z}_T)^2}{\sigma_t^2} \right) \right] \\ &= \exp \left[ -\frac{1}{2} \left( \left( \frac{a_t^2}{\delta_t^2} + \frac{1}{\sigma_{t-1}^2} \right) \mathbf{z}_{t-1}^2 - 2 \left( \frac{a_t b_t \mathbf{z}_T}{\delta_t^2} + \frac{m_{t-1}\mathbf{z}_0 + n_{t-1}\mathbf{z}_T}{\sigma_{t-1}^2} \right) \mathbf{z}_{t-1} + C(\mathbf{z}_t, \mathbf{z}_0, \mathbf{z}_T) \right) \right]. \end{aligned} \quad (17)$$

where  $C(\mathbf{z}_t, \mathbf{z}_0, \mathbf{z}_T)$  indicates the constant term that is independent of  $\mathbf{z}_{t-1}$ . Since the Gaussian distribution probability density  $\mathbf{z}_{t-1} \sim \mathcal{N}(\tilde{\boldsymbol{\mu}}_t, \tilde{\sigma}_t^2\mathbf{I})$  can be expressed in the following form:

$$\exp \left( -\frac{(\mathbf{z}_{t-1} - \tilde{\boldsymbol{\mu}}_t)^2}{2\tilde{\sigma}_t^2} \right) = \exp \left[ -\frac{1}{2} \left( \frac{1}{\tilde{\sigma}_t^2} \mathbf{z}_{t-1}^2 - \frac{2\tilde{\boldsymbol{\mu}}_t}{\tilde{\sigma}_t^2} \mathbf{z}_{t-1} + \frac{\tilde{\boldsymbol{\mu}}_t^2}{\tilde{\sigma}_t^2} \right) \right]. \quad (18)$$

We can thus derive:

$$\begin{aligned} \frac{1}{\tilde{\sigma}_t^2} &= \frac{a_t^2}{\delta_t^2} + \frac{1}{\sigma_{t-1}^2} \\ \Rightarrow \tilde{\sigma}_t^2 &= \frac{\sigma_{t-1}^2(\sigma_t^2 - a_t^2\sigma_{t-1}^2)}{\sigma_t^2} = \frac{\sigma_{t-1}^2}{\sigma_t^2} \delta_t^2 \end{aligned} \quad (19)$$

$$\begin{aligned} \frac{\tilde{\boldsymbol{\mu}}_t}{\tilde{\sigma}_t^2} &= \frac{a_t \mathbf{z}_t - a_t b_t \mathbf{z}_T}{\delta_t^2} + \frac{m_{t-1} \mathbf{z}_0 + n_{t-1} \mathbf{z}_T}{\sigma_{t-1}^2} \\ \Rightarrow \tilde{\boldsymbol{\mu}}_t &= \left[ \frac{\sigma_{t-1}^2 (a_t \mathbf{z}_t - a_t b_t \mathbf{z}_T) + \delta_t^2 (m_{t-1} \mathbf{z}_0 + n_{t-1} \mathbf{z}_T)}{\delta_t^2 \sigma_{t-1}^2} \right] \frac{\sigma_{t-1}^2}{\sigma_t^2} \delta_t^2 \\ &= \frac{\sigma_{t-1}^2}{\sigma_t^2} a_t \mathbf{z}_t + \frac{\delta_t^2}{\sigma_t^2} m_{t-1} \mathbf{z}_0 + \left( \frac{\delta_t^2}{\sigma_t^2} n_{t-1} - \frac{\sigma_{t-1}^2}{\sigma_t^2} a_t b_t \right) \mathbf{z}_T \end{aligned} \quad (20)$$

whose results are equivalent to Equation (6) and Equation (7).

Accordingly, maximizing the Evidence Lower Bound (ELBO) is equivalent to minimizing the KL divergence between ground truth and predicted posterior:

$$\begin{aligned} &KL(q(\mathbf{z}_{t-1} | \mathbf{z}_0, \mathbf{z}_t, \mathbf{z}_T) || p_\theta(\mathbf{z}_{t-1} | \mathbf{z}_t, \mathbf{z}_T)) \\ &= \mathbb{E}_{q(\mathbf{z}_{t-1} | \mathbf{z}_0, \mathbf{z}_t, \mathbf{z}_T)} \left[ \log \frac{\frac{1}{\sqrt{2\pi\tilde{\sigma}_{t-1}}} e^{-\frac{(\mathbf{z}_{t-1} - \tilde{\boldsymbol{\mu}}_{t-1})^2}{2\tilde{\sigma}_{t-1}^2}}}{\frac{1}{\sqrt{2\pi\tilde{\sigma}_{\theta,t-1}}} e^{-\frac{(\mathbf{z}_{t-1} - \tilde{\boldsymbol{\mu}}_{\theta,t-1})^2}{2\tilde{\sigma}_{\theta,t-1}^2}}} \right] \\ &= \mathbb{E}_{q(\mathbf{z}_{t-1} | \mathbf{z}_0, \mathbf{z}_t, \mathbf{z}_T)} \left[ \log \tilde{\sigma}_{\theta,t-1} - \log \tilde{\sigma}_{t-1} - \frac{(x_{t-1} - \tilde{\boldsymbol{\mu}}_{t-1})^2}{2\tilde{\sigma}_{t-1}^2} + \frac{(x_{t-1} - \tilde{\boldsymbol{\mu}}_{\theta,t-1})^2}{2\tilde{\sigma}_{\theta,t-1}^2} \right] \\ &= \log \frac{\tilde{\sigma}_{\theta,t-1}}{\tilde{\sigma}_{t-1}} - \frac{1}{2} + \frac{\tilde{\sigma}_{t-1}^2}{2\tilde{\sigma}_{\theta,t-1}^2} + \frac{(\tilde{\boldsymbol{\mu}}_{t-1} - \tilde{\boldsymbol{\mu}}_{\theta,t-1})^2}{2\tilde{\sigma}_{\theta,t-1}^2} \end{aligned} \quad (21)$$

If we assume that only the mean term is learnable during training, and  $\tilde{\sigma}_{\theta,t-1} = \tilde{\sigma}_{t-1}$ , we can ignore all the unlearnable constants and arrive at the final training objective:

$$\begin{aligned} \mathcal{L} &= \mathbb{E}_{t, \mathbf{z}_0, \mathbf{z}_t, \mathbf{z}_T} \left[ \frac{1}{2\tilde{\sigma}_t^2} \|\tilde{\boldsymbol{\mu}}_{t-1} - \tilde{\boldsymbol{\mu}}_{\theta,t-1}(\mathbf{z}_t, \mathbf{z}_T, t)\|^2 \right] \\ &= \mathbb{E}_{t, \mathbf{z}_0, \mathbf{z}_t, \mathbf{z}_T} \left[ \|\boldsymbol{\epsilon} - \boldsymbol{\epsilon}_\theta(\mathbf{z}_t, \mathbf{z}_T, t)\|^2 \right] \end{aligned} \quad (22)$$

which is the same as in Equation (8) and Equation (9). This concludes our derivation.

## B. Experiments

### B.1. Network Architecture

The basic structure of our network follows the original design of Stable Diffusion. To better utilize visual information ( $\mathbf{z}_T$  in our case), we concatenating both intermediate samples and input image along the feature dimension and send in the noise prediction network as a whole. To address the dimension incompatibility with pretrained backbone, the input channels of the network are thus doubled to accommodate the concatenated input. In addition, as suggested by (Ke et al., 2024), we duplicate the weight tensor of these accommodated layers and divide the values by two to preserve the input magnitude to subsequent layers. As DPBridge is an image-conditioned generative framework, we employ null-text embedding for all cross-attention layers to eliminate the impact of text prompts.

### B.2. Additional Quantitative Results

In this section, we further evaluate the robustness of DPBridge system by perturbing the input image with different types and different level intensities of noise. In this experiment setting, we use Stable Diffusion 1.5 as pretrained backbone. The

evaluation is conducted using under both depth estimation and surface normal prediction tasks. We use NYUv2 and KITTI to report the depth estimation results, as for surface normal prediction, we report the results on NYUv2 and iBims-1. Table 4 reveals that the model’s performance degrades as noise intensity increases, but the model performance remains acceptable under moderate-level-intensity noise. Among noise types, uniform noise shows the mildest effect on degradation, while salt & pepper and high-intensity gaussian noise cause the most significant performance decline. In addition, the noise intensity has more impact on surface normal prediction than depth estimation, showcasing the inherent characteristics between different tasks. These results emphasize the model’s robustness under moderate noise but still expose its vulnerability to extreme or specific types of noise.

Noise Type	Noise Level	Depth Estimation				Surface Normal Prediction			
		NYUv2		KITTI		NYUv2		iBims-1	
		AbsRel↓	$\delta_1$ ↑	AbsRel↓	$\delta_1$ ↑	Mean↓	11.25° ↑	Mean↓	11.25° ↑
<b>Original Version</b>	-	6.9	95.7	11.2	87.3	18.1	54.2	24.3	51.2
<b>Gaussian</b>	$\mathcal{N}(0, 0.05)$	7.2	94.4	11.8	86.0	18.6	52.2	25.6	45.1
	$\mathcal{N}(0, 0.1)$	8.4	92.7	12.1	85.3	20.3	49.4	27.4	40.4
	$\mathcal{N}(0, 0.2)$	10.3	90.0	15.7	78.6	24.6	43.7	37.0	25.4
	$\mathcal{N}(0, 0.5)$	15.9	77.2	22.5	67.1	41.3	22.5	50.0	13.2
<b>Uniform</b>	$\mathcal{U}(-0.05, 0.05)$	7.0	95.0	11.4	86.5	18.3	53.6	24.5	50.7
	$\mathcal{U}(-0.1, 0.1)$	7.2	94.7	11.5	85.4	18.7	53.0	24.8	49.4
	$\mathcal{U}(-0.2, 0.2)$	7.6	94.0	12.0	85.0	19.5	50.5	26.0	46.1
	$\mathcal{U}(-0.5, 0.5)$	9.3	91.1	16.3	76.1	22.4	42.2	30.2	31.6
<b>Poisson</b>	$Poisson(\lambda = 0.05)$	10.2	90.2	13.1	82.5	21.3	45.6	28.1	38.9
	$Poisson(\lambda = 0.1)$	11.8	88.9	15.4	79.3	23.2	40.3	34.9	24.8
<b>Salt &amp; Pepper</b>	<i>Probability=5%</i>	12.0	85.4	13.3	81.7	26.3	28.8	31.8	29.6
	<i>Probability=10%</i>	14.3	82.2	16.0	76.2	28.6	26.3	35.3	21.4

Table 4: Robustness evaluation on depth estimation and surface normal prediction tasks with different types and different intensities of noise. During all experiments, the input images are normalized between -1 to 1.

### B.3. Additional Qualitative Results

To further validate the effectiveness and generalization of DPBridge, we provide qualitative results for various dense prediction tasks, including semantic segmentation, optical flow prediction, and style transfer, by framing them as continuous-valued image-to-image translation problems. For semantic segmentation, we convert discrete labels into color maps and use our bridge model to predict colors in RGB space instead of categorical labels. For optical flow, the bridge process is defined between the flow image and the first image in the input RGB pair. To accommodate this, we adapt the UNet architecture to incorporate both RGB images as conditions during inference and convert the flow map into RGB space, predicting corresponding colors rather than uv coordinates. The following figures (Figure 6, Figure 7, Figure 8, Figure 9) illustrate that DPBridge achieves visually satisfactory results across different tasks. Note that only qualitative assessments are presented here; detailed implementations and quantitative evaluations are left as directions for future research.

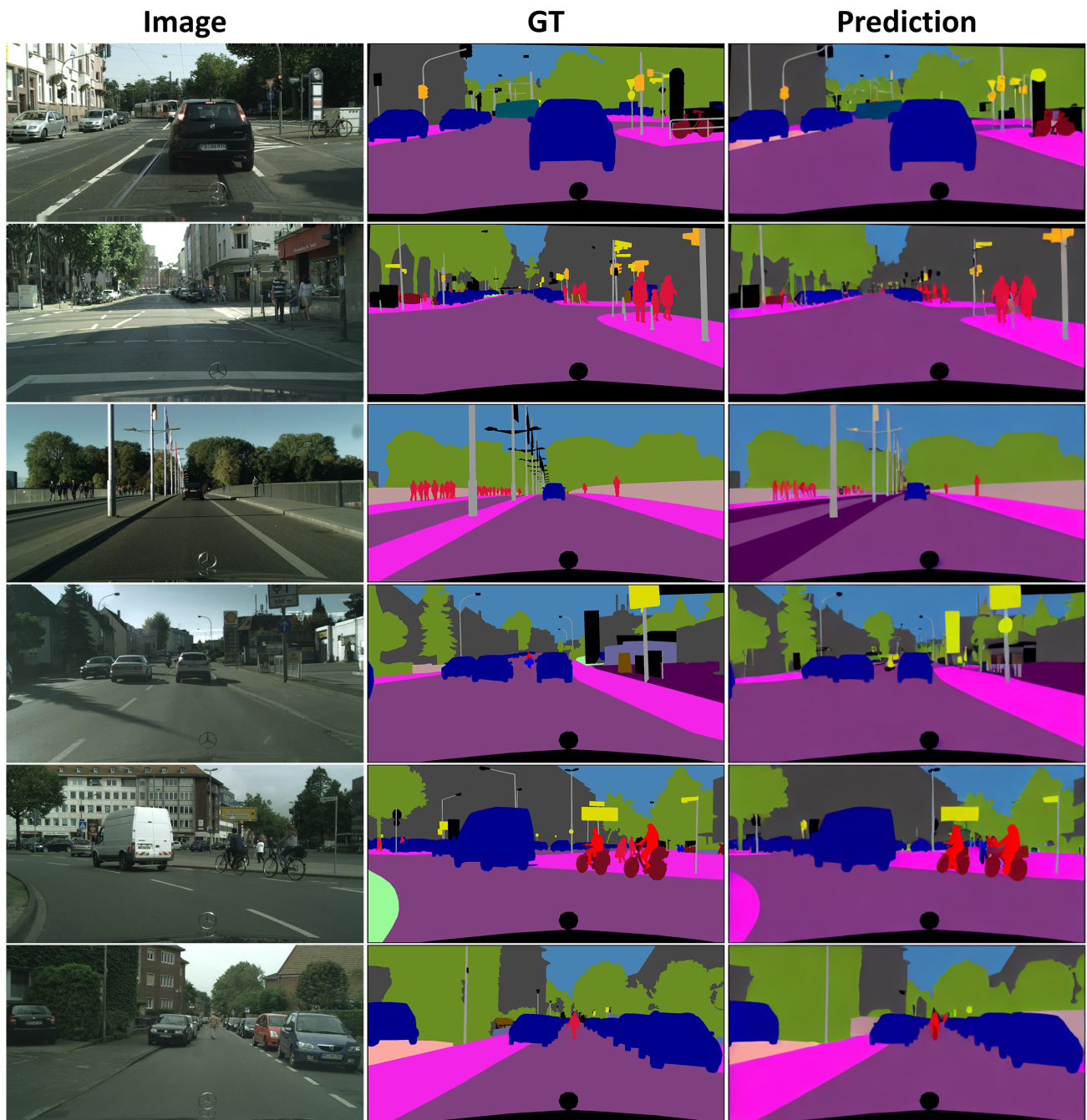


Figure 6: Qualitative examples of applying DPBridge to semantic segmentation task on CityScape (Cordts et al., 2016) dataset. We transform discrete labels into color maps and use our bridge model to predict colors in RGB space instead of categorical labels.

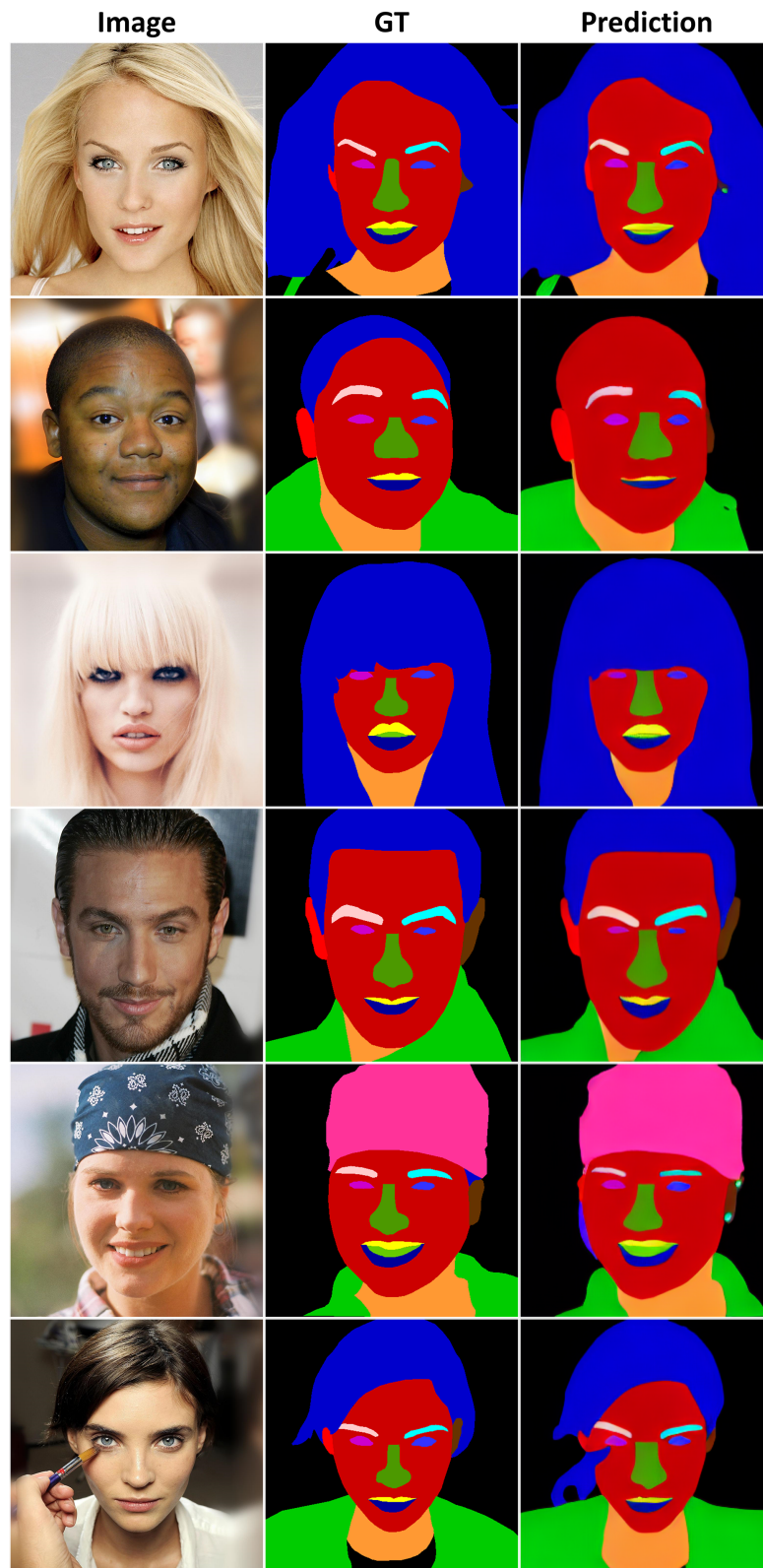


Figure 7: Qualitative examples of applying DPBridge to semantic segmentation task on CelebAMask-HQ (Lee et al., 2020) dataset. We transform discrete labels into color maps and use our bridge model to predict colors in RGB space instead of categorical labels.

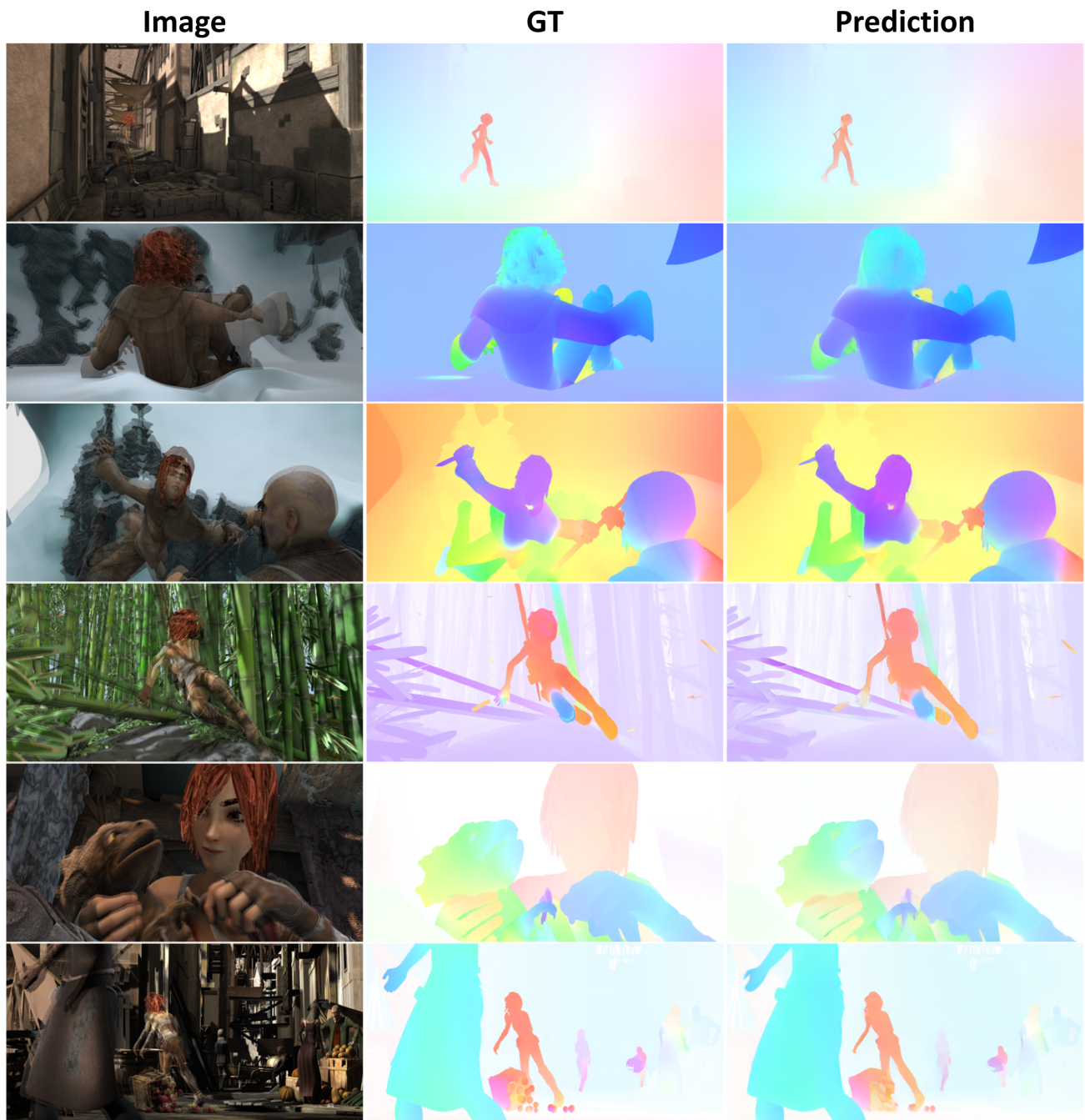


Figure 8: Qualitative examples of applying DPBridge to optical flow prediction task on MPI-Sintel (Butler et al., 2012) dataset. The input image is the overlaid RGB pair, and we transform the flow map into RGB space so that the diffusion bridge process can be constructed accordingly.

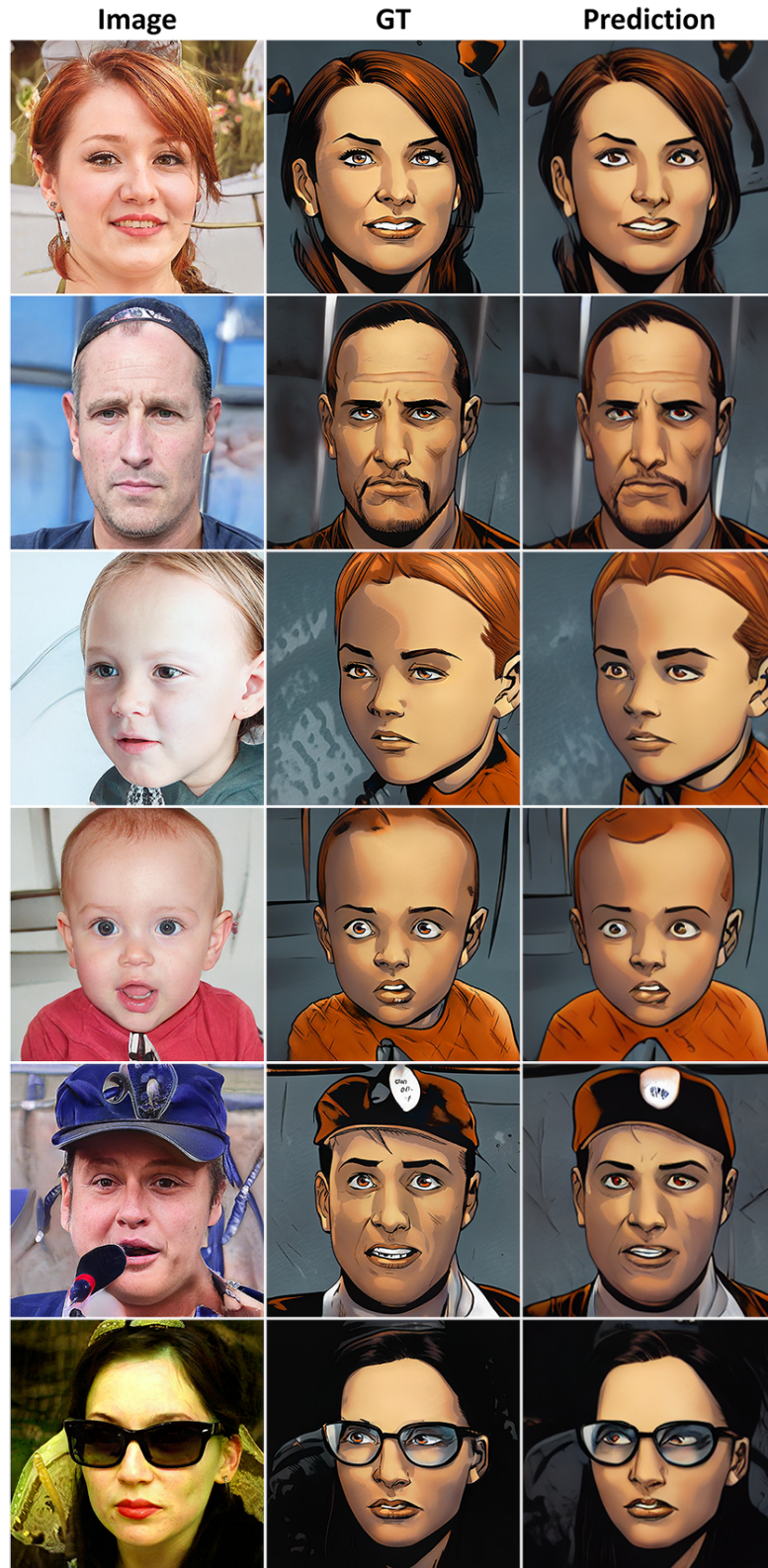


Figure 9: Qualitative examples of applying DPBridge to style transfer task on Face-to-Comics (Sxela, 2021) dataset.